REGION GROWING: ADOLESCENCE AND ADULTHOOD

Two Visions of Region Growing: in Feature Space and Variational Framework

C. Revol-Muller[1], T. Grenier[1], J. L. Rose[1], A. Pacureanu[1], F. Peyrin[2] and C. Odet[1]
[1]*CREATIS, CNRS UMR 5220, Inserm U1044, Univ. de Lyon 1, INSA-Lyon, 7 Av. Jean Capelle 69621, Lyon, France*
[2]*ESRF, BP 220, 38043 Grenoble Cedex, France*

Keywords: Region Growing, Feature Space, Scale Parameters, Variational Approach, Shape Prior Energy, Vesselness.

Abstract: Region growing is one of the most intuitive techniques for image segmentation. Starting from one or more seeds, it seeks to extract a meaningful object by iteratively aggregating surrounding pixels. Starting from this simple description, we propose to show how region growing technique can be elevated to the same rank as more recent and sophisticated methods. Two formalisms are presented to describe the process. The first one derived from non-parametric estimation relies upon feature space and kernel functions. The second one is issued from variational framework. Describing the region evolution as a process, which minimizes an energy functional, it thus proves the convergence of the process and takes advantage of the huge amount of work already done on energy functional. In the last part, we illustrate the interest of both formalisms in the context of life imaging. Three segmentation applications are considered using various modalities such as whole body PET imaging, small animal μCT imaging and experimental Synchrotron Radiation μCT imaging. We will thus demonstrate that region growing has reached this last decade a maturation that offers many perspectives of applications to the method.

1 INTRODUCTION

Life imaging by means of many modalities (X-ray Computed Tomography, Magnetic Resonance Imaging (MRI), Ultrasounds, Positron Emission Tomography (PET), etc.) allows a three-dimensional exploration of the anatomical structures with an increasingly precision and provides to the doctors or biologists a huge amount of data to analyse. In order to leverage these high-tech imaging systems, it is of the utmost importance to have efficient software to automatically extract the objects of interest. This process called "image segmentation" is fundamental, since it conditions the quality of the ulterior study, in terms of accuracy of measurements and quantitative analysis carried on the explored anatomical structures. Image segmentation is a strenuous problem, especially in life imaging, due to complexity of the anatomical objects, weak spatial resolution, special nature of the physical processes involved in the formation of the images as well as presence of noise and specific artefacts according to the imaging modalities and the imaged structures (artefacts of movement, physical artefacts of interface, inhomogeneity of the background....).

Since the first definition of segmentation given by Zucker in "Region Growing: Childhood and adolescence" (Zucker, 1976), many techniques have been proposed in literature to solve the problem: region growing (Adams and Bischof, 1994; Mehnert and Jackway, 1997; Revol and Jourlin, 1997; Chuang and Lie, 2001; Grenier *et al.*, 2007), snakes and active contours (Kass *et al.*, 1987; Xu and Prince, 1998; Paragios and Deriche, 2002; Freedman and Zhang, 2004) , level sets (Malladi *et al.*, 1995; Paragios and Deriche, 2005), graph cuts (Boykov and Jolly, 2001; Rother *et al.*, 2004), etc.

Among region-based approaches, region growing is often used in semi-interactive segmentation software. This technique is appreciated by the users for its simple, flexible and intuitive use. Generally, it consists in extracting a region of interest by aggregating all the neighbouring pixels considered as homogeneous, starting from an initial set of seeds created manually (Olabarriaga and Smeulders, 2001) or automatically (Lin *et al.*, 2000; Fan *et al.*, 2001). The criterion of homogeneity is evaluated from the grey levels of the region (statistical moments, parameters of texture, Bayesian approaches).

However, the main disadvantage of region

Revol-Muller C., Grenier T., Rose J., Pacureanu A., Peyrin F. and Odet C..
REGION GROWING: ADOLESCENCE AND ADULTHOOD - Two Visions of Region Growing: in Feature Space and Variational Framework.
DOI: 10.5220/0003942002860297
In *Proceedings of the International Conference on Computer Vision Theory and Applications* (VISAPP-2012), pages 286-297
ISBN: 978-989-8565-03-7

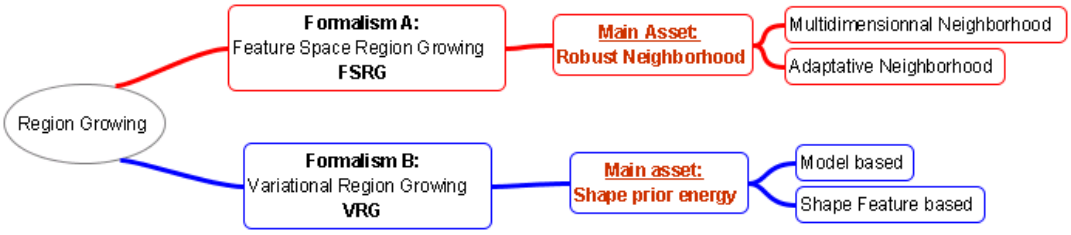

Figure 1: Two formalisms of region growing process.

growing is to be badly affected by unwanted spread or leak outside the sought object since the process cannot distinguish connected structures with similar intensities or statistic properties. In order to solve problems due to objects connectivity, the integration of geometrical constraints during the growth is essential. Whereas some techniques are well suitable to take into account shape prior (Cremers *et al.*, 2003; Gastaud *et al.*, 2004; Chan and Zhu, 2005; Foulonneau *et al.*, 2006), region growing in its original description is not supported by a mathematical framework that could help it to do so, and thus sparse solutions are mainly ad-hoc (Dehmeshki *et al.*, 2003; Rose *et al.*, 2007).

In this paper, we propose to underpin region growing by means of two formalisms (see Figure 1). The first formalism is feature space oriented. It allows to process whatever kind of data (e.g. grey levels, physical parameters, spatial coordinates). Its major advantage is to define a robust neighbourhood i.e a set of points belonging to the targeted population without considering outliers. Furthermore, this approach allows to describe adaptive approach since the neighbourhood can be locally adjusted to the variation of the underlying probability density of data. We will demonstrate the interest of this approach by describing a multidimensional and an adaptive region growing. The second formalism describes region growing in a variational framework. The region growing is viewed as an iterative and convergent process driven by an energy minimization. This formalism is especially useful to take into account whatever kind of energy based on different types of information e.g. contour, region or shape. We will illustrate this approach by detailing two solutions for integrating shape prior in region growing: i) via a model-based energy and ii) via a feature shape energy.

In Section 4, we show that region growing can be successfully used in the context of experimental life imaging. We present segmentation results in a wide range of applications starting from NaF PET images, small animal CT-imaging and also SRμCT imaging. We will thus demonstrate that by means of these two formalisms, region growing can be easily designed to positively answer to the needs of the applications.

2 FORMALISM A: FEATURE SPACE REGION GROWING (FSRG)

In this formalism, region growing aims to segment points that belong to a multidimensional space called feature space. We call this approach FSRG. The number of features used to describe a point determines the dimension of this space. This approach is especially useful in the context of medical imaging, where data to process come from multimodality imaging like PET-CT devices or from maps of physical parameters such as ρ, T1, T2 in MRI or echogenicity, elasticity, diffusors density in ultrasound imaging. In FSRG, region growing seeks to group similar points together by using techniques stemmed from non-parametric density estimation based on kernel function. After some definition reminders, we set up the principle of FSRG.

2.1 Definitions

2.1.1 Region

A region R (resp. $\bar{R}$) is the set of the segmented (resp. non-segmented) points of a d-dimensional space $\mathbf{R}^d$. As region growing is an iterative process, the content of a region at an iteration t is noted $R^{[t]}$. The initial region $R^{[0]}$ is usually called the set of seeds.

FSRG formalism derives from the framework of non-parametric density estimation based on kernel function (for further details, see (Silverman, 1986)) which consists in reconstructing the underlying density of multidimensional data by means of $\mathbf{K}_\mathbf{H}$ a multidimensional kernel function normalized by $\mathbf{H}$ a matrix of scaled parameters as reminds in (1):

$$\hat{f}(\mathbf{x};\mathbf{H}) = \frac{1}{n}\sum_{i=1}^{n} K_\mathbf{H}(\mathbf{x}-\mathbf{x}_i) \quad (1)$$

2.1.2 Kernel

In FSRG, K also denotes a kernel function but with weaker constrains than in (1) (especially, no normalization requirement):

$$K(\mathbf{x}):\begin{cases}\mathbf{R}^d \to [0,1] \\ K(\vec{0}) = Max(K(\mathbf{x})) \\ K(\vec{\infty}) \to 0\end{cases} \quad (2)$$

For convenience, a profile k can be associated to K a radially symetric kernel:

$$K(\mathbf{x}) = k(\mathbf{x}^T\mathbf{x}) \quad (3)$$

In particularly, the special profile k_{rect} will be used:

$$k_{rect}(u) = \begin{cases}1 & if \quad |u| \le 1 \\ 0 & otherwise\end{cases} \quad u \in \mathbf{R}^+ \quad (4)$$

In our case, u corresponds to a squared distance between two points in the feature space such as:

$$d_M^2(\mathbf{x},\mathbf{y},\mathbf{H}) = (\mathbf{x}-\mathbf{y})^T\,\mathbf{H}^{-1}(\mathbf{x}-\mathbf{y}) \quad (5)$$

also called the Mahalanobis distance, where $\mathbf{H}$ the matrix of scaled parameters, is symetric and positive-definite. If $\mathbf{H}$ is chosen diagonal, the computed distance is called the normalized Euclidian distance.

The points $\mathbf{x} \in \mathbf{R}^d$ can be separated in c subvectors $\mathbf{x}_j$ associated to their c features $\left(j \in [1,c]\right)$. The matrix $\mathbf{H}$ can samely decomposed in c submatrix $\mathbf{H}_j$:

$$\mathbf{H} = \begin{bmatrix}\mathbf{H}_1 & & 0 \\ & \ddots & \\ 0 & & \mathbf{H}_c\end{bmatrix} \quad (6)$$

Then, a multidimensional kernel built from a product of spheric kernels can be expressed as a product of unidimensional kernels K_j:

$$K_{\mathbf{H}}(\mathbf{x}) = \prod_{j=1}^{c} K_j\left(\left(\mathbf{x}_j^T(\mathbf{H}_j)^{-1}\mathbf{x}_j\right)^{1/2}\right)$$
$$K_{\mathbf{H}}(\mathbf{x}) = \prod_{j=1}^{c} k_j\left(\left(\mathbf{x}_j^T(\mathbf{H}_j)^{-1}\mathbf{x}_j\right)\right) \quad (7)$$

By convention, s (resp. r) index will represent spatial (resp. range) feature.

2.1.3 Robust Neighbourhood

We call $N(\mathbf{y})$ the robust neighbourhood of a point $\mathbf{y}$, the set of points that contains all those, which satisfy a special condition and lets apart the outliers.

$$N(\mathbf{y}) = \left\{\mathbf{x} \in X \;\middle|\; k_{rect}\left(d^2(\mathbf{x},\mathbf{y},\mathbf{H})\right) = 1\right\} \quad (8)$$

where X is a subset of $\mathbf{R}^d$ such as: $X \subset \mathbf{R}^d$.

This writing is powerful since it allows to deals with data represented in a feature space through a distance associated to each feature. Moreover, similarly to non-parametric estimation, the scale parameters can be adapted to each point of the space by means of a local matrix $\mathbf{H}_{|\mathbf{y}}$.

For instance, in case of spatial and range features, the adaptive robust $N(\mathbf{y})$ can be written as a product of profiles with adaptative scale parameters:

$$N(\mathbf{y}) = \left\{\mathbf{x} \in X \;\middle|\; k_{rect}\left(d^2\left(\mathbf{x}_s,\mathbf{y}_s,\mathbf{H}_{s|\mathbf{y}}\right)\right) . k_{rect}\left(d^2\left(\mathbf{x}_r,\mathbf{y}_r,\mathbf{H}_{r|\mathbf{y}}\right)\right) = 1\right\} \quad (9)$$

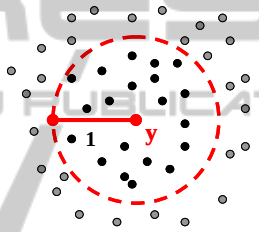

Figure 2: Robust neighbourhood N(y) represented by the set of black points.

2.2 Principle of FSRG

2.2.1 Iterative Process

Region growing is an iterative process that aims to agglomerate new points to an existing region while a special condition is checked. The set of new points at each iteration will be denoted $B^{[t]}$ since this set is spatially included in a narrow band around the current région $R^{[t]}$. Starting from an initial region $R^{[0]}$, the evolution process can be described by (10):

$$R^{[t+1]} = R^{[t]} \cup B^{[t]} \quad (10)$$

This step is repeated until convergence, i.e. the current region does not evolve anymore: $R^{[t+1]} = R^{[t]}$.

2.2.2 Narrow Band $B^{[t]}$

The set $B^{[t]}$ is tightly related to the notion of robust neighbourhood previously defined in section 2.1. It can be defined as the set of points $\{\mathbf{y}\}$, which do not belong to $R^{[t]}$, but whose robust neighbourhood $N(\mathbf{y})$ contains at least a point of $R^{[t]}$.

$$B^{[t]} = \left\{ \mathbf{y} \in \overline{R}^{[t]} \middle| N(\mathbf{y}) \cap R^{[t]} \neq \varnothing \right\} \quad (11)$$

It can be noted that the selection of the new points and the behaviour of the region growing rely entirely upon the robust neighbourhoods $N(\mathbf{y})$.

In the next section, we take advantage of the open formalism of FSRG to describe two kinds of region growing: i) a n-dimensional region growing and ii) a locally adaptive region growing.

2.3 Two Illustrations of FSRG

In the following, the definition of the narrow band $B^{[t]}$ (11) and the principle of evolution (10) stay identical; the methods differ only by their specific robust neighbourhood.

2.3.1 Multidimensional Region Growing (MRG)

The description of a multidimensional region growing as mentioned in (Comaniciu and Meer, 2002) is straightforward with FSRG. The multidimensional kernel used in the robust neighbourhood can process both spatial and range features of the set *X*.

$$N(\mathbf{y}) = \left\{ \mathbf{x} \in X \middle| k_{rect}\left(d^2(\mathbf{x}_s, \mathbf{y}_s, \mathbf{H}_s)\right) . k_{rect}\left(d^2(\mathbf{x}_r, \mathbf{y}_r, \mathbf{H}_r)\right) = 1 \right\} \quad (12)$$

$N(\mathbf{y})$ contains the points spatially close to $\mathbf{y}$ and with a range feature similar to $\mathbf{y}_r$. The maximum extents are controlled by the matrix $\mathbf{H}_s$ and $\mathbf{H}_r$.

2.3.2 Adaptive Region Growing (ARG)

In (Grenier *et al.*, 2007), the authors present a Robust Adaptive Region Growing (Road RG) which can be rewritten within FSRG framework. This method integrates local information about the average gray levels of near points belonging to $R^{[t]}$ and the average norm of the gradient in some vicinity of the tested point (see Figure 3). Thus, the robust neighbourhood can take the following form:

$$N(\mathbf{y}) = \left\{ \mathbf{x} \in X \middle| k_{rect}\left(d^2(\mathbf{x}_s, \mathbf{y}_s, \mathbf{H}_s)\right) . k_{rect}\left(d^2(\mathbf{x}_r, \mathbf{y}_r, \mathbf{H}_{r|\mathbf{y}})\right) = 1 \right\} \quad (13)$$

The scale parameters in matrix $\mathbf{H}_s$ are constant for the spatial features but those of the matrix $\mathbf{H}_{r|\mathbf{y}}$ for

Figure 3: Local information used in Road RG.

the range features are adapted to each point $\mathbf{y}$. In the context of RoAd RG, the range feature is one-dimensional, so $\mathbf{H}_{r|\mathbf{y}}$ is simply a scalar value updated for each point $\mathbf{y}$. This value can be easily determined from the adaptive range of the tolerate variation presented in the paper.

To sum up, FSRG is a useful formalism which unifies many region growing approaches previously presented in the litterature. Furthermore, the description in feature space widens the possibilites of region growing which is not restricted anymore to a segmentation method dedicated to grey level images. The robust neighbourhood grounded on kernel density estimation leverages the technique and offers many advantages such as the ability to describe adaptive approach by means of scale parameters.

In the next section, we present a second formalism for region growing which profits from the powerful variational framework.

3 FORMALISM B: VARIATIONAL REGION GROWING (VRG)

Variational Region Growing formalism (VRG) describes the region growing as an optimization process that aims to minimize some functional called energy, by analogy with many physics phenomena. It relies upon the hypothesis that for an energy judiciously chosen, the segmented region corresponds to pixels that minimizes the energy. This approach is widely used in many segmentation techniques e.g. Bayesian segmentation, active contours, level sets,, graph-cuts, but thus far, not fully capitalized by region growing (Adams and Bischof, 1994; Zhu and Yuille, 1996; Revol-Muller *et al.*, 2002; Grenier *et al.*, 2007; Rose *et al.*, 2007). It was only in 2009 that VRG was firstly described in literature by (Rose *et al.*, 2009b; Rose *et al.*, 2010).

3.1 Definitions

3.1.1 Region Representation

The evolving region is represented by a characteristic function $\Phi_{\mathbf{x}}$ defined as:

$$\Phi_{\mathbf{x}} = \Phi(\mathbf{x}) = \begin{cases} 1, & if \ \mathbf{x} \in \Omega_{in} \\ 0, & if \ \mathbf{x} \in \Omega_{out} \end{cases} \quad (14)$$

where $\mathbf{x} \in \mathbf{R}^d$ is an element of the image domain Ω, Ω_{in} the subset representing the segmented region in Ω and $\Omega_{out} = \Omega \setminus \Omega_{in}$ the absolute complement of Ω_{in} representing the background.

The initial region $(t = 0)$ is described by the characteristic function Φ^0:

$$\Phi^0 = \{\mathbf{x} \in \Omega \,|\, \Phi(\mathbf{x}, t = 0) = 1\} \quad (15)$$

3.1.2 ε-Neighbourhood

The ε-neighbourhood of a point $\mathbf{u}$ of the metric space Ω is the set of all points close to $\mathbf{u}$ in accordance with Euclidian distance:

$$N_{\varepsilon}(\mathrm{u}) = \{v \in \Omega \,|\, \|v - u\| \le \varepsilon\} \quad (16)$$

The outer (resp. inner) boundary δ_{ε}^{+} (resp. δ_{ε}^{-}) of Ω_{in} is defined as follows:

$$\begin{aligned} \partial_{\varepsilon}^{+} &= \{v \in \Omega_{out} \,|\, \exists u \in \Omega_{in},\ v \in N_{\varepsilon}(u)\} \\ \partial_{\varepsilon}^{-} &= \{v \in \Omega_{in} \,|\, \exists u \in \Omega_{out},\ v \in N_{\varepsilon}(u)\} \end{aligned} \quad (17)$$

The union of inner and outer boundaries can also be noted $\delta_{\varepsilon}^{\pm}$.

3.2 Principle of VRG

VRG aims to achieve the desired image partition by switching the discrete function $\Phi_{\mathbf{x}}$, in order to minimize an energy functional which models the structure to detect. Of course, this energy functional must be correctly designed in such a way that its minimum corresponds to the solution of the segmentation i.e the sought object.

3.2.1 Segmentation by Variational Approach

In a variational approach, the segmentation is expressed as an optimisation process:

$$\Phi^* = \arg\min_{\Phi} J(\Phi) \quad (18)$$

where Φ^* is the optimal partition of image obtained by minimizing the energy $J(\Phi)$.

In order to iteratively find the solution, an artificial time-variable t is introduced, thus allowing to relate $\Delta_t \Phi$ the time-dependent variation of Φ with $\Delta J(\tilde{\Phi})$ the estimated variation of the energy for $\tilde{\Phi}$ a small alteration of Φ as follows:

$$\Delta_t \Phi + F(\Phi, \Delta J(\tilde{\Phi})) = 0 \quad (19)$$

where F is a functional controlling the region evolution.

3.2.2 Equation of Evolution

In VRG, the evolution of the region is a discrete process in both spatial and time domains because elements of Ω are sampled on a grid and iterations depend on a discrete-time variable n.

In this case, the aim of F is to induce the switch of Φ values, each time that yields a reduction of the energy i.e. $\Delta J(\tilde{\Phi}) < 0$. Thus, F can be expressed as a function of $\Delta J(\tilde{\Phi})$ and $c(\Phi)$ the switch state command expressed in (22), as follows:

$$F(\Phi, \Delta J(\tilde{\Phi})) = -c(\Phi) \cdot H(-\Delta J(\tilde{\Phi})) \quad (20)$$

where H stands for the one-dimensional Heaviside function:

$$H(z) = \begin{cases} 0 & if \ z < 0 \\ 1 & if \ z \ge 0 \end{cases} \quad (21)$$

The command $c(\Phi)$ leads to the switch of $\Phi_{\mathbf{x}}$ at a point $\mathbf{x}$ by means of the next operation:

$$c(\Phi_{\mathbf{x}}) = 1 - 2\Phi_{\mathbf{x}} \quad (22)$$

From (19) and (20) the evolution of the region can be written as:

$$\Delta_t \Phi - c(\Phi) \cdot H(-\Delta J(\tilde{\Phi})) = 0 \quad (23)$$

The equation (23) is solved iteratively by numerical methods starting from Φ^0. We note Φ^n the region function at iteration n. The values of the function Φ at the iteration $n+1$ are evaluated at each point as follows:

$$\Phi_{\mathbf{x}}^{n+1} = \Phi_{\mathbf{x}}^{n} + c(\Phi_{\mathbf{x}}^{n}) \cdot H(-\Delta J(\tilde{\Phi}_{\mathbf{x}}^{n})) \quad (24)$$

Depending on the sign of $\Delta J(\tilde{\Phi}_{\mathbf{x}}^{n})$, the value of $\Phi_{\mathbf{x}}^{n+1}$ is switched or remains unchanged. The

evolution stops when Φ^n does not encounter any modification at the assessed points.

3.2.3 Vicinity to Assess

In VRG, at each iteration, only a limited set of voxels are evaluated for possible aggregation. These voxels are selected by defining a vicinity which surrounds the boundary of the segmented region. The width of this vicinity depends on the size of the ε-neighbourhood (16) used to defined the outer and inner boundaries (17). The aim of this vicinity is similar to the narrow band used in level sets. Most of the time, only the outer boundary is considered for the evolution of the region. However, if the inner boudary is included in the vicinity, that means that points belonging previously to the evolving region can be tested at the next iteration and possibly ejected. The vicinity is taken into account in the equation of evolution (24) by replacing $c(\Phi_{\mathbf{x}}^n)$ by $c_\varepsilon(\Phi_{\mathbf{x}}^n)$.

$$c_\varepsilon(\Phi_{\mathbf{x}}^n) = \begin{cases} c(\Phi_{\mathbf{x}}^n) & \text{if } \mathbf{x} \in \delta_\varepsilon^{\pm} \\ 0 & \text{otherwise} \end{cases} \quad (25)$$

3.2.4 Energy Variation

Since the evolution of the region depends on the energy variation $\Delta J(\tilde{\Phi}_{\mathbf{x}}^n)$, it is of interest to find out a common expression of this variation for a wide class of energies. Among the plethora of energies proposed in the literature, we restrict the study on region-based energies. In (Jehan-Besson *et al.*, 2003), the author presents a general expression of a region-based energy obtained from a "region-independent" descriptor $k_{\mathbf{x}}$ as:

$$J(\Omega_{in}) = \int_{\Omega_{in}} k_{\mathbf{x}} d\mathbf{x} \quad (26)$$

In our discrete case, the expression of the energy becomes:

$$J(\Phi^n) = \sum_{\mathbf{x}\in\Omega} k_{\mathbf{x}} \Phi_{\mathbf{x}}^n \quad (27)$$

Given the energy $J\left(\Phi^n\right)$ at the iteration *n*, we evaluate the energy $J\left(\tilde{\Phi}^n\right)$ that would result from the state switch of a candidate voxel $\mathbf{v}$.

The assessed state switch of $\mathbf{v}$ is defined by:

$$\tilde{\Phi}_v^n = 1 - \Phi_v^n \quad (26)$$

Thus:

$$\tilde{\Phi}_{\mathbf{x}}^n = \Phi_{\mathbf{x}}^n \quad \text{if } \mathbf{x} \neq \mathbf{v} \quad (29)$$

From the relations (27), (28), (29) the evaluated energy can be then written as:

$$J(\tilde{\phi}^n) = k_v \cdot \tilde{\phi}_v^n + \sum_{\mathbf{x}\neq v, \mathbf{x}\in\Omega} k_{\mathbf{x}} \cdot \phi_{\mathbf{x}}^n \quad (30)$$

$$J(\tilde{\Phi}^n) = k_{\mathbf{v}} \cdot \left(1 - \Phi_{\mathbf{v}}^n\right) - k_{\mathbf{v}} \cdot \Phi_{\mathbf{v}}^n + \underbrace{k_{\mathbf{v}} \cdot \Phi_{\mathbf{v}}^n + \sum_{\mathbf{x}\neq\mathbf{v}} k_{\mathbf{x}} \cdot \Phi_{\mathbf{x}}^n}_{J(\Phi^n)} \quad (31)$$

Therefore, the energy variation $\Delta J\left(\tilde{\Phi}_{\mathbf{v}}^n\right)$, associated to a single voxel $\mathbf{v}$ have the following formulation:

$$\Delta J\left(\tilde{\Phi}_{\mathbf{v}}^n\right) = \left(1 - 2\Phi_{\mathbf{v}}^n\right) \cdot k_{\mathbf{v}} \quad (32)$$

This expression for the evolution of the energy functional is valid for any region-independent descriptor $k_{\mathbf{v}}$.

3.2.5 Example of Region-based Energy

In (Chan and Vese, 2001), the authors propose a region-based energy based on the average grey level calculated inside and outside the segmented region:

$$J_{CV}(\Phi_{\mathbf{x}}) = \lambda_{\text{int}} \sum_{\mathbf{x}} \left| f(\mathbf{x}) - \mu_{in} \right|^2 \Phi_{\mathbf{x}} + \lambda_{ext} \sum_{\mathbf{x}} \left| f(\mathbf{x}) - \mu_{out} \right|^2 \left(1 - \Phi_{\mathbf{x}}\right) \quad (33)$$

Where μ_{in} (resp. μ_{out}) is the average intensity in Ω_{in} (resp. Ω_{out}) and $f\left(\mathbf{x}\right)$ the intensity value of the pixel $\mathbf{x}$.

According to (32), the variation of this energy expresses as following:

$$\Delta J_{CV}\left(\tilde{\Phi}_{\mathbf{v}}^n\right) = \left(1 - 2\Phi_{\mathbf{v}}^n\right)\left[\left| f(\mathbf{v}) - \mu_{in} \right|^2 - \left| f(\mathbf{v}) - \mu_{out} \right|^2\right] \quad (34)$$

To sum up the section 3.2, VRG formalism describes region growing as an iterative process that converges towards a minimum of energy. VRG is a powerful formalism since it allows to deal with whatever kind of energies. The next section presents two solutions to constrain region growing by shape prior: i) from a model-based energy and ii) from a feature shape energy.

3.3 Integration of Shape Prior

3.3.1 Model-based Energy

The definition of a model-based energy is

conceivable when a reference shape is available. This approach was successfully implemented by (Foulonneau *et al.*, 2006; Rose *et al.*, 2009a). It consists in describing the shape by descriptors such as Legendre or Chebyschev moments. Then, a shape distance based on these descriptors must be carefully defined in order to compare the shape of the evolving region with the one of the reference object. The shape energy governing the region growing will be tightly related to this distance.

In the following, we briefly remind the approach proposed by (Rose *et al.*, 2009a) that relies on a shape energy based on Chebyschev moments.

a. Chebyschev moments

The Chebyschev moments of order $\eta=(p+q)$ of a binary image of size N defined by a characteristic function $\Phi_{\mathbf{x}}$ are expressed using the scaled orthogonal Chebyschev polynomials $t_{p,N}(.)$, as follows:

$$T_{pq}=C_{pq}\cdot\sum_{\mathbf{x}\in\Omega}t_{p,N}(x_1)t_{q,N}(x_2)\Phi_{\mathbf{x}} \qquad p,q=0,1,2,..,\eta-1 \tag{35}$$

where the p-th order Chebyschev polynomial is given by:

$$t_{p,N}(x_1)=\frac{p!}{N^p}\sum_{k=0}^{p}(-1)^{p-k}\binom{N-1-k}{p-k}\binom{p+k}{p}\binom{x_1}{k} \tag{36}$$

These moments are made invariant by using an affine transformation T^{aff} such as $\mathbf{u}=T^{\text{aff}}\mathbf{x}$ where $\mathbf{u}=[u_1,u_2]$, thus allowing shape alignment during the segmentation

$$\nu_{pq}=C_{pq}\cdot\sum_{\mathbf{x}\in\Omega}t_{p,N}(u_1)t_{q,N}(u_2)\Phi_{\mathbf{x}} \tag{37}$$

b. Shape prior energy

The shape prior energy is based on the weighted Frobenius distance. It measures the difference between the set of moments describing the inside of the evolving region Φ^n and the set of moments of the reference object.

$$J_{prior}(\Phi^n)=\sum_{p,q}^{p,q<\eta}H_{pq}(\sigma)^2\cdot\left(T_{pq}(\Phi^n)-T_{pq}^{ref}\right)^2 \tag{38}$$

where H_{pq} is a weighting positive function used to adapt the criterion to the Chebyschev moment hierarchy:

$$H_{pq}(\sigma)=\frac{1}{\sqrt{2\pi\sigma^2}}\exp^{-\frac{(p+q)^2}{2\sigma^2}} \tag{39}$$

c. Variation of the shape prior energy

The principle used to determine the variation of energy $\Delta J(\tilde{\Phi}_{\mathbf{v}}^n)$ is the same than 3.2.4. The variation at the voxel $\mathbf{v}$ is given by the following equation:

$$\Delta J_{prior}(\tilde{\Phi}_{\mathbf{v}}^n)=(1-2\Phi_{\mathbf{v}}^n)\cdot\sum_{p,q}^{p+q<\eta}2T_{pq}^nR_{\mathbf{v}}+(1-2\Phi_{\mathbf{v}}^n)R_{\mathbf{v}}^2-2T_{pq}^{ref}R_{\mathbf{v}} \tag{40}$$

where $R_{\mathbf{v}}=C_{pq}t_{p,N}(u_1)t_{q,N}(u_2)$.

Depending on the sign of $\Delta J(\tilde{\Phi}_{\mathbf{v}}^n)$ value, the region function Φ^n will evolve by aggregating or rejecting a point belonging to the vicinity of Φ^n.

d. Total energy

In order to define a process of segmentation that depends on both grey levels of the image and shape prior given by the reference model, a mixed energy $J_T(\Phi_{\mathbf{x}})$ must be introduced in VRG:

$$J_T(\Phi_{\mathbf{x}})=J_I(\Phi_{\mathbf{x}})+\alpha*J_{prior}(\Phi_{\mathbf{x}}) \tag{41}$$

with $J_I(\Phi_{\mathbf{x}})$ the energy of Chan and Vese presented in (33) and $J_{prior}(\Phi_{\mathbf{x}})$ the shape prior-energy defined in equation (38). The hyper-parameter α balances the influence of shape prior and image data.

The variation of the total energy at the voxel $\mathbf{v}$ will take into account the variation of each energy:

$$\Delta J_T(\tilde{\Phi}_{\mathbf{v}}^n)=\Delta J_I(\tilde{\Phi}_{\mathbf{v}}^n)+\alpha*\Delta J_{prior}(\tilde{\Phi}_{\mathbf{v}}^n) \tag{42}$$

In the next section, another kind of shape prior energy is proposed. This energy derives from special shape features of the sought structure.

3.3.2 Energy based on Shape Features

The energy based on a shape feature is defined by a functional, which takes into account some information on the geometry of the structure to detect. For instance, the structure of the object can be mainly tubular. Such an energy is presented in (Pacureanu *et al.*, 2010), the authors propose to introduce vesselness information in the energy

functional in order to improve the spread of the region growing into tubular structures.

The vesselness information is obtained by a special filtering based on Hessian matrix (Frangi *et al.*, 1998; Sato *et al.*, 1998), which yields a probability map of the tubular-like structures in the image. The filter can be tuned to enhance tubular features of a particular size.

The energy functional $J_{FS}(\Phi_{\mathbf{x}})$ combines $f(\mathbf{x})$ the intensity information in the original image and $v(\mathbf{x})$ the vesselness information obtained from Sato or Frangi filtered image. Each term of the energy is weighted by the likelihood that the current element belongs to a tubular structure, which is given by the value of $v(\mathbf{x})$.

$$J_{FS}(\Phi_{\mathbf{x}}) = J_f(\Phi_{\mathbf{x}}) + J_v(\Phi_{\mathbf{x}}) \tag{43}$$

where

$$\begin{aligned} J_v(\Phi_{\mathbf{x}}) &= \sum_{\mathbf{x}} v(\mathbf{x}) \left| v(\mathbf{x}) - \mu_{v_{in}} \right|^2 \Phi_{\mathbf{x}} \\ &+ \sum_{\mathbf{x}} v(\mathbf{x}) \left| v(\mathbf{x}) - \mu_{v_{out}} \right|^2 (1 - \Phi_{\mathbf{x}}) \end{aligned} \tag{44}$$

$$\begin{aligned} J_f(\Phi_{\mathbf{x}}) &= \sum_{\mathbf{x}} (1 - v(\mathbf{x})) \left| f(\mathbf{x}) - \mu_{f_{in}} \right|^2 \Phi_{\mathbf{x}} \\ &+ \sum_{\mathbf{x}} (1 - v(\mathbf{x})) \left| f(\mathbf{x}) - \mu_{f_{out}} \right|^2 (1 - \Phi_{\mathbf{x}}) \end{aligned} \tag{45}$$

with $v(\mathbf{x})$ the vesselness similarity measure at the voxel $\mathbf{x}$ and $\mu_{v_{in}}, \mu_{v_{out}}$ (respectively $\mu_{f_{in}}, \mu_{f_{out}}$) the average grey levels of the domains Ω_{in} and Ω_{out} in the filtered image $v(\mathbf{x})$ (respectively in the original image $f(\mathbf{x})$).

The variation of the energy functional at the voxel $\mathbf{v}$ expresses as follows:

$$\Delta J_{FS}(\tilde{\Phi}^n_{\mathbf{v}}) = (1 - 2\Phi^n_{\mathbf{v}}) \left(k_{\mathbf{v}}(J_v) + k_{\mathbf{v}}(J_f) \right) \tag{46}$$

where

$$k_{\mathbf{v}}(J_v) = v(\mathbf{v}) \left(\left| v(\mathbf{v}) - \mu_{v_{in}} \right|^2 - \left| v(\mathbf{v}) - \mu_{v_{out}} \right|^2 \right) \tag{47}$$

$$k_{\mathbf{v}}(J_f) = (1 - v(\mathbf{v})) \left(\left| f(\mathbf{v}) - \mu_{f_{in}} \right|^2 - \left| f(\mathbf{v}) - \mu_{f_{out}} \right|^2 \right) \tag{48}$$

$v(\mathbf{v}) \in [0,1]$ can be seen as a measure of the probability of the voxel $\mathbf{v}$ to be part of a tube-like structure. During the segmentation evolution, when a tested voxel belongs to a tubular structure $v(\mathbf{v})$ is close to 1, therefore, the term $k_{\mathbf{v}}(J_v)$ in the equation (46) is preponderant. If the considered voxel is part of the background or of non-tubular structure, $v(\mathbf{v})$ is close to 0 and the term $k_{\mathbf{v}}(J_f)$ becomes preponderant, hence the intensity in the original image is taken into account. As we will see in the section 4.3, this energy permits to detect both lacunae and canaliculi and, by propagation on the line enhancement provided by Sato's filter, it makes possible to reconnect parts of the same canaliculus.

4 APPLICATIONS TO MEDICAL AND BIOMEDICAL IMAGING

In this section, we illustrate the use of region growing in the context of life imaging. Three region growing methods derived from FSRG and VRG formalisms were applied to segment images from various modalities such as whole body PET images, small animal µCT images and SRµCT images of caniculae network.

4.1 FSRG ARG: Whole body PET Images of Bone Activity

4.1.1 [^{18}F]Fluoride Ion PET Images

Figure 4a displays an example of a whole body [^{18}F]fluoride ion PET study, obtained with a standard protocol of [^{18}F]fluoride ion PET acquisition described in (Grenier *et al.*, 2005). The dimensions of the volume are 128x128x349 pixels and the grey levels are coded in short format (16 bits). The intensity values are proportional to the tracer uptake.

Through the plots of two profiles, Figure 4d and Figure 4e highlight the high variations of the intensity and the strong inhomogeneity of the tracer uptake due to bone metabolism. The yellow line and curve used for the profiles were drawn on the same slice located in the skull (Figure 4b and Figure 4c).

4.1.2 Results

In this application, the aim is to segment the skull and the spinal column in whole body [^{18}F]fluoride ion PET studies. The adaptive region growing ARG described in (2.3.2) was chosen to perform this segmentation due to its ability to adapt to the local inhomogeneity of the signal by means of its local scale parameter.

ARG was compared to a non-adaptive region growing method NARG, thus defined: tested voxels are agglomerated if their grey levels belong to a

predetermined range of variation around the mean gray level of the evolving region. In both methods, the initial seeds were automatically set up by a procedure described in (Grenier et al., 2005).

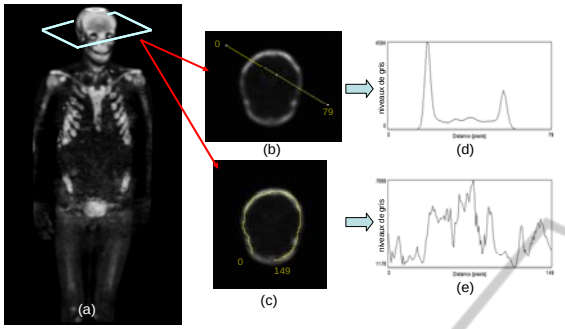

Figure 4: (a) Whole body [18F]fluoride ion PET image; (b), (c) the same slices in the skull; (d), (e) two profiles of intensity.

Figure 5c and Figure 5d display the results of the segmentation with NARG and ARG. For both methods, tuning parameters were experimentally adjusted. In the skull, ARG leads to a better segmentation than NARG, since the evolving region has successfully spread over the whole structure despite the high variations of the intensities. That demonstrates the improvements provided by the use of the adaptive parameters.

4.2 VRG-model-based Energy: Application to µCT Images of Mice Kidney

VRG driven by a model-based energy (3.3.1) was applied to segment three dimensional micro-CT scans of mice kidney (Rose *et al.*, 2009a). The framework of the application is the phenotyping of mice kidneys. The 3D reference model was obtained by a previous manual segmentation of a reference volume. The method was tested on a random input volume. Slices of x-plane and y-plane are shown in Figure 6a and Figure 6d.

We compare the results of VRG with and without shape prior i.e using $J_T(\Phi_{\mathbf{x}})$ or only $J_I(\Phi_{\mathbf{x}})$. Figure 6b, Figure 6e and Figure 7a show the resulting segmentation without shape prior $(\alpha = 0)$. The segmentation fails to segment the kidney due to strong inhomogeneities in the image. Moreover, the final contour spreads through the leaking points induced by an artifact.

Figure 6c, Figure 6f and Figure 7b illustrate VRG results with shape prior constraint. The

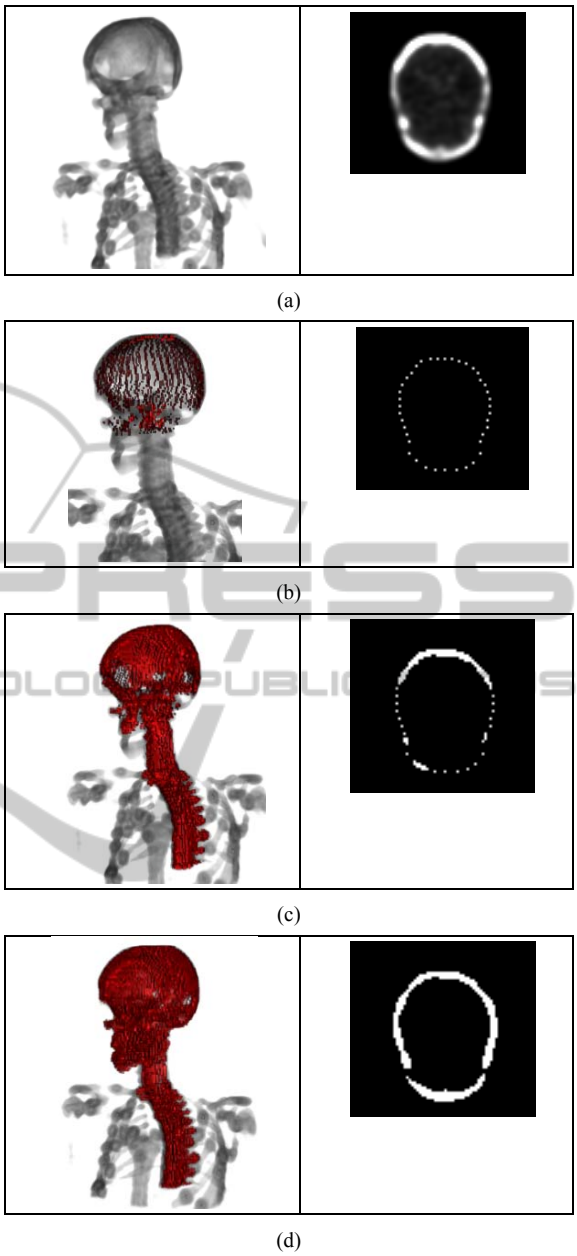

Figure 5: Segmentation of [18F]fluoride ion PET image: a) original data, b) initial seeds, c) NARG results, d) ARG results. For each column, 3D representation is given in the left and a slice located in the skull is given in the right.

parameter σ stepping in $J_{prior}(\Phi_{\mathbf{x}})$ was set to 1.5. This value was not chosen too low in order to take into account enough information about the reference model. The hyper-parameter α was fixed to 200 and achieves a good compromise between $J_{prior}(\Phi_{\mathbf{x}})$ and $J_I(\Phi_{\mathbf{x}})$ since the kidney surface has been recovered more accurately and without any leakage.

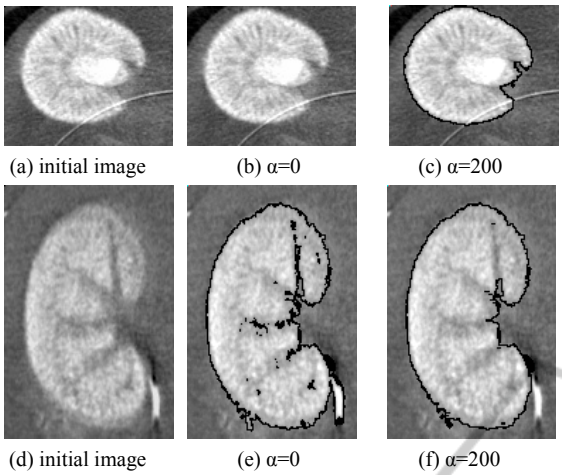

Figure 6: μ -CT image segmentation: (a,d) slices of the input volume, (b, e) segmentation result without shape prior, (c, f) segmentation result with the model-based shape prior.

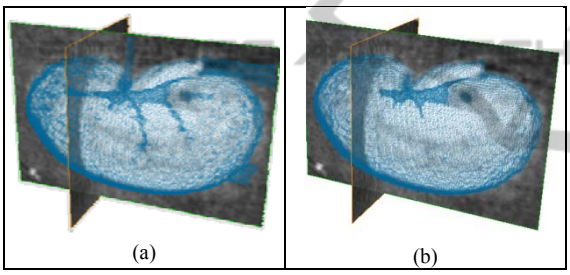

Figure 7: Segmentation results: a) without shape prior; b) with model-based shape prior.

4.3 VRG-feature Shape Energy: Application to SRμCT Images of Canaliculi Network

VRG driven by a feature shape energy (3.3.2) was applied to segment experimental data obtained with very high resolution SR-μCT at ESRF, representing 3D images of the lacuno-canalicular structure in human femur bone tissue. For the sample presented in Figure 8, the acquisition resolution was 0.28μm, the energy was set at 20.5keV and 2000 projections were taken with a counting time of 0.8 seconds. The osteocyte cell network is essentially composed of ellipsoidal objects interconnected through tubular structures. The main difficulty in segmenting this formation arises from the slender canaliculi, the linear features occupying only a few voxels in diameter.

The vesselness map was created by applying Sato's filter on the original image. This process enhances 3D curvilinear structures in the filtered image. The seeds for the initialization of the region growing were obtained by thresholding the vesselness map. The parameters used for the vesselness filter were determined from a previous study based on a phantom.

Figure 8 displays the results obtained for a 800x500x100 sub-volume extracted from a $(2048)^3$ volume. Figure 8a shows a Maximum Intensity Projection of the original sub-volume. Figure 8b VRG has efficiently yielded the first segmentation results of the canalicular system, in 3D from SR-μCT.

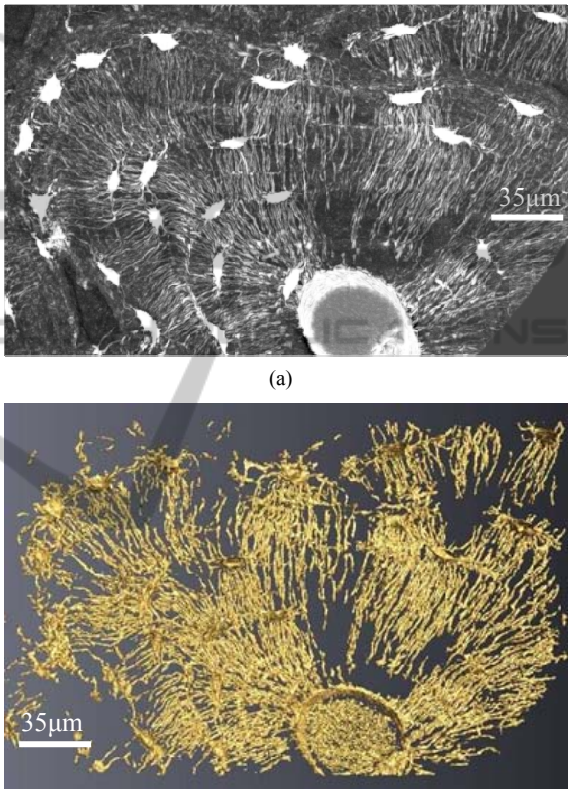

Figure 8: Volume of interest showing the lacuno-canalicular system in a human femur bone sample (image width ~ 224 μm): a) Maximum Intensity Projection of the original (inverted) volume; b) Isosurface of the segmentation obtained with VRG and the feature shape energy $J_{FS}(\Phi_{\mathbf{x}})$.

Moreover, it has been demonstrated in a quantitative study carried on simulated data (Pacureanu *et al.*, 2010) that VRG driven by the shape feature energy $J_{FS}(\Phi_{\mathbf{x}})$ over performs VRG only driven by $J_I(\Phi_{\mathbf{x}})$, since it can detect correct tubular structures at a rate 20% higher and lead to better connection of the caniculi network.

5 CONCLUSIONS

We have presented two visions of region growing. The first one can easily deal with multidimensional data in the feature space and specify locally adaptive segmentation. The second one leverages the powerful mathematical tools of variational framework. One major advantage is to bring convergence properties through the minimization of the energy functional.

Various approaches derived from both formalisms have been successfully applied to life imaging, yielding quite satisfying results while enabling simple initializations, intuitive interactions and easy understanding of tuning parameters by users. From our knowledge, these two formalisms should encompass whatever region growing approaches proposed in the literature.

ACKNOWLEDGEMENTS

The authors thank the ESRF ID19 group for help during data acquisition and Pr. M Lafage-Proust (Inserm U890, St Etienne, France) for providing the bones samples.

REFERENCES

Adams R, Bischof L, 1994. Seeded region growing. *IEEE Transactions on Pattern Analysis and Machine Intelligence,* 16, 641-7.

Boykov Y Y, Jolly M P, 2001. Interactive graph cuts for optimal boundary and region segmentation of objects in N-D images. In: *8th IEEE International Conference on Computer Vision, Vol I, Proceedings*, 105-12.

Chan T, Zhu W, 2005. Level set based shape prior segmentation. In: *Proceedings - 2005 IEEE Computer Society Conference on Computer Vision and Pattern Recognition, CVPR 2005*, 1164-70.

Chan T F, Vese L A, 2001. Active contours without edges. *IEEE Transactions on Image Processing,* 10, 266-77.

Chuang C H, Lie W N, 2001. Region growing based on extended gradient vector flow field model for multiple objects segmentation. In: *IEEE International Conference on Image Processing*, 74-7.

Comaniciu D, Meer P, 2002. Mean shift: A robust approach toward feature space analysis. *IEEE Transactions on Pattern Analysis and Machine Intelligence,* 24, 603-19.

Cremers D, Sochen N, Schnörr C, 2003. Towards recognition-based variational segmentation using shape priors and dynamic labeling. *Scale Space Methods in Computer Vision,* 2695/2003, 388-400.

Dehmeshki J, Ye X, Costello J, 2003. Shape based region growing using derivatives of 3D medical images: Application to semi-automated detection of pulmonary nodules. In: *IEEE International Conference on Image Processing*, 1085-8.

Fan J, Yau D K Y, Elmagarmid A K, Aref W G, 2001. Automatic image segmentation by integrating color-edge extraction and seeded region growing. *IEEE Transactions on Image Processing,* 10, 1454-66.

Foulonneau A, Charbonnier P, Heitz F, 2006. Affine-invariant geometric shape priors for region-based active contours. *Pattern Analysis and Machine Intelligence, IEEE Transactions on,* 28, 1352-7.

Frangi A F, Niessen W J, Vincken K L, Viergever M A, 1998. Multiscale vessel enhancement filtering. In: *Medical Image Computing and Computer-Assisted Intervention - Miccai'98*, 130-7.

Freedman D, Zhang T, 2004. Active contours for tracking distributions. *IEEE Transactions on Image Processing,* 13, 518-26.

Gastaud M, Barlaud M, Aubert G, 2004. Combining shape prior and statistical features for active contour segmentation. *Circuits and Systems for Video Technology, IEEE Transactions on,* 14, 726-34.

Grenier T, Revol-Muller C, Costes N, Janier M, Gimenez G, 2005. Automated seeds location for whole body NaF PET segmentation. *IEEE Trans. Nuc. Sci.,* 52, 1401-5.

Grenier T, Revol-Muller C, Costes N, Janier M, Gimenez G, 2007. 3D robust adaptive region growing for segmenting [18F] fluoride ion PET images. In: *IEEE Nuclear Science Symposium Conference Record*, 2644-8.

Jehan-Besson S, Barland M, Aubert G, 2003. DREAM2S: Deformable regions driven by an Eulerian accurate minimization method for image and video segmentation. *International Journal of Computer Vision,* 53, 45-70.

Kass M, Witkin A, Terzopoulos D, 1987. Snakes: active contour models. In: *Proceedings - First International Conference on Computer Vision.*, 259-68.

Lin Z, Jin J, Talbot H, 2000. Unseeded region growing for 3D image segmentation. *ACM International Conference Proceeding Series, 2000.*

Malladi R, Sethian J A, Vemuri B C, 1995. Shape modeling with front propagation: a level set approach. *IEEE Transactions on Pattern Analysis and Machine Intelligence,* 17, 158-75.

Mehnert A, Jackway P, 1997. Improved seeded region growing algorithm. *Pattern Recognition Letters,* 18, 1065-71.

Olabarriaga S D, Smeulders A W M, 2001. Interaction in the segmentation of medical images: A survey. *Medical Image Analysis,* 5, 127-42.

Pacureanu A, Revol-Muller C, Rose J L, Sanchez-Ruiz M, Peyrin F, 2010. A Vesselness-guided Variational Segmentation of Cellular Networks from 3D Micro-CT. In: *IEEE International Symposium on Biomedical Imaging: From Nano to Macro*, 912 - 5.

Paragios N, Deriche R, 2002. Geodesic active regions: A new framework to deal with frame partition problems in computer vision. *Journal of Visual Communication*

and Image Representation, 13, 249-68.

Paragios N, Deriche R, 2005. Geodesic active regions and level set methods for motion estimation and tracking. *Computer Vision and Image Understanding,* 97, 259-82.

Revol-Muller C, Peyrin F, Carrillon Y, Odet C, 2002. Automated 3D region growing algorithm based on an assessment function. *Pattern Recognition Letters,* 23, 137-50.

Revol C, Jourlin M, 1997. New minimum variance region growing algorithm for image segmentation. *Pattern Recognition Letters,* 18, 249-58.

Rose J L, Grenier T, Revol-Muller C, Odet C, 2010. Unifying variational approach and region growing segmentation. In: *18th European Signal Processing Confernce (EUSIPCO-2010)*, 1781-5.

Rose J L, Revol-Muller C, Almajdub M, Chereul E, Odet C, 2007. Shape Prior Integrated in an Automated 3D Region Growing method. In: *IEEE International Conference on Image Processing ICIP'07*, 53-6.

Rose J L, Revol-Muller C, Charpigny D, Odet C, 2009a. Shape prior criterion based on Tchebichef moments in variational region growing. In: *IEEE International Conference on Image Processing ICIP'09*, 1077-80.

Rose J L, Revol-Muller C, Reichert C, Odet C, 2009b. Variational region growing. In: *VISAPP-09 International Conference on Computer Vision Theory and Applications*, 166-71.

Rother C, Kolmogorov V, Blake A, 2004. "GrabCut" - Interactive foreground extraction using iterated graph cuts. *Acm Transactions on Graphics,* 23, 309-14.

Sato Y, Nakajima S, Shiraga N, Atsumi H, Yoshida S, Koller T, Gerig G, Kikinis R, 1998. Three-Dimensional Multi-Scale Line Filter for Segmentation and Visualization of Curvilinear Structures in Medical Images. *Medical Image Analysis,* 2, 143-68.

Silverman B W, 1986. *Density Estimation for Statistiques and Data Analysis* vol 26 (London)

Xu C, Prince J L, 1998. Generalized gradient vector flow external forces for active contours. *Signal Processing,* 71, 131-9.

Zhu S C, Yuille A, 1996. Region competition: unifying snakes, region growing, and Bayes/MDL for multiband image segmentation. *IEEE Transactions on Pattern Analysis and Machine Intelligence,* 18, 884-900.

Zucker S W, 1976. Region growing: Childhood and adolescence. *Computer Graphics and Image Processing,* 5, 382-99.